Path integral Monte Carlo on a lattice. II. Bound states

Mark O'Callaghan and Bruce N. Miller
Department of Physics and Astronomy, Texas Christian University, Fort Worth, Texas 76129, USA
(Received 25 June 2015; revised manuscript received 6 May 2016; published 18 July 2016)

The equilibrium properties of a single quantum particle (qp) interacting with a classical gas for a wide range of temperatures that explore the system's behavior in the classical as well as in the quantum regime is investigated. Both the qp and the atoms are restricted to sites on a one-dimensional lattice. A path integral formalism developed within the context of the canonical ensemble is utilized, where the qp is represented by a closed, variable-step random walk on the lattice. Monte Carlo methods are employed to determine the system's properties. To test the usefulness of the path integral formalism, the Metropolis algorithm is employed to determine the equilibrium properties of the qp in the context of a square well potential, forcing the qp to occupy bound states. We consider a one-dimensional square well potential where all atoms on the lattice are occupied with one atom with an on-site potential except for a contiguous set of sites of various lengths centered at the middle of the lattice. Comparison of the potential energy, the energy fluctuations, and the correlation function are made between the results of the Monte Carlo simulations and the numerical calculations.

DOI: 10.1103/PhysRevE.94.012120

I. INTRODUCTION

This paper explores the physics of one-dimensional systems in which a single low-mass particle interacts with more massive atoms arranged in some configuration. The mass of the single particle is sufficiently low to require the laws of quantum mechanics, whereas the more massive atoms can be expressed classically. Electrons, positrons, and positronium are some examples of such quantum particles. This general problem is important for studying any situation which can be modeled by an excess or solvated electron in a classical gas, liquid, or solid. Examples include electron transport in insulating materials as well as modeling the nature of weakly ionized plasmas [1]. It is furthermore applicable to lifetime studies of positrons produced by radioactive sources which have been injected into various materials [2]. These are examples of an individual quantum particle (qp) interacting with a configuration of more massive classical atoms. In the limit of infinite classical particle mass, we are compelled to consider the idealized geometry where all particles are fixed in space and both the atoms and qp are restricted to sites on a regular lattice.

In this study we leverage off the work performed by O'Callaghan and Miller [3], which we refer to as "Paper 1" from now on, where a general approach was developed to solve for the equilibrium properties for quenched one-dimensional systems for any configuration of atoms. This paper incorporated the tight-binding model combined with a specially developed imaginary-time path integral Monte Carlo (PIMC) algorithm to be employed on lattice problems to solve the system density matrix. As a point of reference, the foundation of the work in Paper 1 is found in Guo and Miller [4].

The tight-binding model is essentially a method to calculate the electronic band structure using an approximate set of wave functions based upon superposition of wave functions for isolated atoms located at each occupied site. The term "tight-binding" refers to the electron being considered tightly bound to the atom in which it is associated such that it has limited interaction with the states of neighboring atoms in the solid [5]. The tight-binding model has been used extensively in the study of many quantum systems including the study of ultracold atoms on optical lattices [6], self-trapping of Bose-Einstein condensates [7], Anderson localization [8], and several studies of graphene [9].

Paper 1 applied the PIMC algorithm for one-dimensional lattice problems to solve for the equilibrium properties for a free qp and for a qp interacting with a potential generated by a so-called striped atomic configuration where every other lattice site is occupied by a classical atom and the other lattice sites are empty. Some of the equilibrium properties considered were the average kinetic energy, the average potential energy, the self-correlation or qp-qp correlation function, and the atom-qp correlation function. These equilibrium properties were studied across a wide range of inverse temperature β. This work showed that the solutions to the Schrödinger equation for the striped case were composed of extended states.

In this same paper a special form of a PIMC algorithm was developed for the one-dimensional lattice problem. When one sees PIMC algorithms in the literature, it is most often for continuous systems. A single qp is replaced by a closed chain of say p pseudoparticles, each interacting with the host system through a p-reduced potential. The predictions are exact in the limit $p \to \infty$ [3]. Path integrals are particularly useful for describing the quantum mechanics of an equilibrium system because the canonical distribution for a single particle in the path integral picture becomes isomorphic with that of a classical ring polymer of quasiparticles [10]. For a continuous system a free particle, whose Hamiltonian is simply the kinetic energy, has a path integral whose integrand is just a product of Gaussians, and hence the positions of the pseudoparticles can always be directly sampled. However, it is almost always the case that when a potential is applied the pseudoparticle positions cannot be directly sampled. The integral has an integrand that is generally not a Gaussian. One then solves the eigenvalue problem for the free particle and constructs a transformation matrix such that the path integral can be described in terms of the normal modes where the kinetic energy Hamiltonian can be directly sampled. The normal modes solutions is then transformed back to pseudoparticle

positions and the Metropolis algorithm is then used to accept or reject the proposed solution based upon the evaluation of the potential energy [11].

We cannot apply the above form of the PIMC algorithm in this problem because the systems considered here involve a qp interacting with a configuration of classical atoms on a rigid one-dimensional lattice, and the particle positions are confined to only be on lattice sites because the space is assumed to be discrete. Thus, the standard assumption of the path integral does not apply. A discrete formulation of a PIMC algorithm was developed in Paper 1. In contrast with other work, here the free particle problem is solved exactly. We actually calculate the matrix elements analytically, and this is not done in other papers. Other works for continuous systems will start with the exact path integral for a free particle, which is a Gaussian [11]. We have proven rigorously that the analog of the Gaussian matrix element in continuous systems is the modified Bessel function in discrete systems. We showed how to construct exact path integrals as a product of these modified Bessel functions. This has not been discovered, explored, or implemented elsewhere in the literature [12].

In this current work, we use the same PIMC algorithm from Paper 1 but apply it to a one-dimensional square well configuration where all lattice sites are occupied by an atom except for a set width of sites focused at the center of the one-dimensional lattice. Here we study three different square well configurations which differ only in well width, which we denote by w, and we focus on the calculations of the same equilibrium properties as [3].

As we stated previously, the striped case paper [3] demonstrated that the solutions to the Schrödinger equation are extended states for that configuration. In this current development, where the atomic configuration is in the form of a one-dimensional square well, we show that the solutions are bound as well as extended states.

Like extended-state quantum-mechanical problems, bound-state quantum-mechanical problems are also a subject of much interest and research. For instance, a popular interaction potential for fluid particles is the square well potential. Fluids modeled in this manner are called "square well fluids." Research of dense fluids often models constituent spherical fluid particles as having a square well interaction [13]. Neutron scattering analyses rely on studying the bound-state energies from a potential approximated by a square well [14]. Furthermore, the study of two-dimensional quantum wires bent into various shapes shows transmission and bound-state energies that are modeled like a square well [15]. Additionally, the interactions between proteins in aqueous solutions is modeled as a square well [16]. Furthermore, many studies of quantum dots model the interacting potential as a square well [17].

The relevance of the application of the square well potential to model atomic, nuclear, and protein interactions has led to researchers performing related in-depth analytical studies. For instance, a thorough analytical investigation was performed by Boykin and Klimeck of individual quantum states [18]. In this paper the discretized Schrödinger equation for a finite square well is analytically solved. They compare and contrast the solutions to this discrete problem with what one typically studies in the continuous case found in many quantum mechanics textbooks. (see, for instance, [19]). They point out that the fundamentally different physics between the discrete and continuous cases arises directly from the finite bandwidth of the discrete model. They argue that a more complete band structure is realized through the application of the discrete model. This then leads to a more accurate physical interpretation, explanation, and description of problems in solid state physics, like modeling the properties of crystals. It is noteworthy to mention that in [18], Boykin and Klimeck stated that only bound states should be found for this square well problem. But, we found extended states as well as bound states.

However, as we demonstrate below, studying the square well potential for a discretized model has relevance to current physics research. Besides this, we would also like to test the efficacy of the subject PIMC code. This was also a goal in Paper 1 where an analytical solution for the striped case was derived, and calculations of some equilibrium properties from the analytical solution were compared with those generated from PIMC computations. For this square well study, we likewise compare the calculations of equilibrium properties derived analytically with those calculated via running the PIMC code. These equilibrium properties include the average kinetic energy, the average potential energy, the qp-qp correlation function, and the atom-qp correlation function. The striped case and square well problems can be done numerically. However, it is important to use the comparison of the PIMC results with analytical or numerical results in order to establish the strengths and weaknesses of the PIMC algorithm before we apply it to cases where an analytical solution is not possible.

The structure of this paper is as follows. In Sec. II we discuss the description of the one-dimensional tight-binding lattice model. In Sec. III, we review the major results of the derivation of equilibrium properties for the free particle on the one-dimensional lattice as derived in the striped case paper [3]. The resulting physical expressions include the forms of the partition function, the average kinetic energy, the average energy fluctuation, the qp-qp correlation function, and the conditional probability for selecting step sizes in the random walk. Also discussed in this section is the atom-qp correlation function and the concept of Metropolis sampling. Then, in Sec. IV, we discuss obtaining the allowed energies for this problem by writing the Schrödinger difference matrix equation and then solving for the eigenvalues and eigenvectors of that matrix. We then discuss how to use this information for calculating system quantities such as the partition function, the average kinetic energy, the average potential energy, the density matrix, the qp-qp correlation function, the atom-qp correlation function and the radius of gyration. We then follow this with a comparison of numerical calculations and corresponding results from runs of the PIMC algorithm. The agreement between numerical and computational results also demonstrates the power of the Monte Carlo method to make physical predictions. Section V then gives the conclusion.

II. DESCRIPTION OF THE MODEL

We study a one-dimensional system of a low-mass qp, like an electron or positron, interacting with a rigid one-dimensional lattice partially occupied with more massive

atoms. In this study, the configuration of the atoms is such that every lattice site will be occupied by one atom except a set of contiguous sites near the center of the lattice. The purpose of this setup is to model a one-dimensional square well potential. We suppose that the temperature is high enough such that the atoms can be treated classically. The space for the quantum particle is discrete; i.e., the quantum particle only lies on the lattice sites. The qp obeys the Schrödinger equation

$$\hat{H}\Psi = E\Psi, \tag{1}$$

where $\hat{H}$ is the Hamiltonian operator, E is the energy eigenvalue, and $|\Psi\rangle$ is the state vector of the qp.

It is convenient to employ second quantization, which possesses the following form for the Hamiltonian operator,

$$\hat{H} = 2t - t\sum_j (c_j^\dagger c_{j+1} + c_{j+1}^\dagger c_j) + \sum_j v_j c_j^\dagger c_j, \tag{2}$$

where c_j is the annihilation operator, $c_j^\dagger$ is the creation operator, and v_j is the potential of the qp on lattice site j. In our model, we simply take

$$v_j = \epsilon n_j, \tag{3}$$

where n_j is the number of atoms on lattice site j, $(n_j = 0, 1)$ and with the choice

$$t = \frac{\hbar^2}{2ma^2}, \tag{4}$$

in which m is the mass of the qp and a is the lattice spacing, we get the discrete approximation of the continuous Hamiltonian. This happens to be the Hamiltonian from the tight-binding model. Without loss of generality, we choose units such that $t = 1$ in all of the following.

III. PATH INTEGRAL FORMALISM

In this paper we study the bound states for a quantum particle interacting with atoms on a one-dimensional lattice where the atoms are arranged in a configuration to form a square well potential. One can always analytically solve for the equilibrium properties for the free quantum particle [3], but in general one can only analytically solve the Schrödinger equation for very few potentials, including the square well potential, the harmonic oscillator potential, the central potential, etc. To solve for equilibrium properties for a quantum system with a general potential, one must rely on a numerical algorithm. For quantum systems, a popular approach is to use a PIMC method.

We follow a PIMC method developed by O'Callaghan and Miller [3], which again we refer to here as "Paper 1." This paper established the framework and method for the PIMC approach where the free particle is represented by a random walk on a one-dimensional lattice that is partially occupied by atoms possessing an on-site potential ϵ. The path integral is isomorphic to a ring polymer with p steps and all of the displacements need to sum to zero to ensure closure. It was shown that the fundamental probability of a sample walk $\mathbf{j} = (j_1, j_2, \ldots, j_p)$ is simply a product of modified Bessel functions of the form

$$\prod_{\alpha=1}^{p} I_{j_\alpha - j_{\alpha+1}}\left(\frac{2\beta t}{p}\right). \tag{5}$$

From this result, Paper 1 then showed derived formulas for the classical analog for the partition function, the average kinetic energy, the mean energy fluctuation, and the qp-qp correlation function for a free particle using the path integral formalism. Below we list the relevant quantities derived in Paper 1 that will be applied to the square well system.

Partition function for a free particle:

$$Z = \mathrm{Tr}[e^{-\beta\hat{H}'}] = \sum_{j_1} \langle j_1 | e^{-\beta\hat{H}'} | j_1 \rangle, \tag{6}$$

where

$$\hat{H}' = \hat{H} - 2t \tag{7}$$

and $\hat{H}$ is the Hamiltonian and t is from Eq. (4).

Path integral estimator of the partition function for a free particle:

$$Z = \sum_{j_1}\sum_{j_2}\cdots\sum_{j_p}\prod_{\alpha=1}^{p} I_{j_\alpha - j_{\alpha+1}}\left(\frac{2\beta t}{p}\right). \tag{8}$$

Kinetic energy for a free particle:

$$\hat{H}' = \hat{T}' = -t\sum_j (c_j^\dagger c_{j+1} + c_{j+1}^\dagger c_j). \tag{9}$$

Path integral estimator for the kinetic energy for a free particle:

$$\hat{\tau} = 2t - \frac{2t}{p}\sum_{\alpha=1}^{p} \frac{I'_{j_\alpha - j_{\alpha+1}}\left(\frac{2\beta t}{p}\right)}{I_{j_\alpha - j_{\alpha+1}}\left(\frac{2\beta t}{p}\right)}. \tag{10}$$

Energy fluctuation for the free particle:

$$\hat{T}'^2 = t^2\left[\sum_j (c_j^\dagger c_{j+1} + c_{j+1}^\dagger c_j)\right]\left[\sum_l (c_l^\dagger c_{l+1} + c_{l+1}^\dagger c_l)\right]. \tag{11}$$

Path integral estimator for the energy fluctuation for a free particle:

$$\tau_2 = \frac{4t^2}{p}\sum_{\alpha=1}^{p} \frac{I''_{j_\alpha - j_{\alpha+1}}\left(\frac{2\beta t}{p}\right)}{I_{j_\alpha - j_{\alpha+1}}\left(\frac{2\beta t}{p}\right)} - \frac{8t^2}{p}\sum_{\alpha=1}^{p} \frac{I'_{j_\alpha - j_{\alpha+1}}\left(\frac{2\beta t}{p}\right)}{I_{j_\alpha - j_{\alpha+1}}\left(\frac{2\beta t}{p}\right)} + 4t^2. \tag{12}$$

qp-qp correlation function for a free particle:

$$\hat{G}_1(n) = \sum_j c_j^\dagger c_{j+n}. \tag{13}$$

Path integral estimator for the qp-qp correlation function for a free particle:

$$\Gamma_1(n) = \frac{1}{p}\sum_{\alpha=1}^{p} \frac{I_{j_\alpha - j_{\alpha+1} - n}\left(\frac{2\beta t}{p}\right)}{I_{j_\alpha - j_{\alpha+1}}\left(\frac{2\beta t}{p}\right)}, \tag{14}$$

where $I_n(z)$ is the modified Bessel function [20] given by

$$I_n(z) = \frac{1}{\pi}\int_0^\pi \mathrm{d}u e^{z\cos u}\cos(nu) \tag{15}$$

and the primes denote differentiation with respect to the inverse temperature β. In the above equations, the j_α represent pseudoparticle positions of the classical ring polymer isomorphism and p is the number of pseudoparticles. Also, the qp-qp correlation function provides a measure of how spread out the quantum particle is on the lattice.

In Paper 1 we show that the free particle paths can be generated from a conditional probability argument that bases the new step $s_{\nu+1}$ on the steps $s_1, s_2, \ldots, s_\nu$ already determined, where $\nu \leqslant p$. It was shown that the resulting probability can be expressed in terms of modified Bessel functions indexed by the steps in the random walk,

$$P(s_{\nu+1}|s_1,s_2,\ldots,s_\nu) = \frac{I_{s_{\nu+1}}\left(\frac{2\beta t}{p}\right) I_{t_{\nu+1}}\left(\frac{p-\nu-1}{p}2\beta t\right)}{I_{t_\nu}\left(\frac{p-\nu}{p}2\beta t\right)}, \quad (16)$$

where

$$t_\nu = \sum_{\alpha=1}^{\nu} s_\alpha, \quad (17)$$

with the step displacement $j_{\alpha+1} - j_\alpha$.

A free particle in a continuous system, whose Hamiltonian is simply the kinetic energy, has a path integral whose integrand is just a product of Gaussians, and hence the positions of the pseudoparticles can always be directly sampled. However, it is almost always the case that when any potential exists in a quantum system, the pseudoparticle positions cannot be directly sampled, simply because the path integral is no longer a product of Gaussians. Under the influence of a potential, the probability of a specific walk on the lattice is proportional to

$$\exp\left(-\frac{\beta V}{p}\right)\left[\prod_{\alpha=1}^{p} I_{s_\alpha}\left(\frac{2\beta t}{p}\right)\right]\Delta\left(\sum_{\alpha=1}^{p} s_\alpha\right), \quad (18)$$

where

$$\Delta(x) = \begin{cases} 1 & x = 0, \\ 0 & x \neq 0. \end{cases} \quad (19)$$

All averages must now include the Gibbs factor $\exp(-\frac{\beta V}{p})$, as well as the product of modified Bessel functions [3]. In contrast with the free particle, for the case of a general interacting system the presence of this factor in the distribution function prevents us from being able to directly sample the probability distribution for the random walk. To deal with this complication, we employ Metropolis sampling. That is, we utilize the free particle conditional probability, as expressed previously, to generate a walk, but we then employ rejection to produce a sequence of walks which satisfies the correct distribution. Let q represent the acceptance factor,

$$q = \frac{\prod_{\alpha=1}^{p} e^{-\beta V'_{j_\alpha}}}{\prod_{\alpha=1}^{p} e^{-\beta V_{j_\alpha}}} = \frac{\exp\left(-\frac{\beta}{p}\sum_{\alpha=1}^{p} V'_{j_\alpha}\right)}{\exp\left(-\frac{\beta}{p}\sum_{\alpha=1}^{p} V_{j_\alpha}\right)}, \quad (20)$$

where V' is the potential energy of the new walk and V is the potential energy of the previous walk. Then, according to the Metropolis criteria, if $q > 1$, we automatically accept the new walk, while if $q < 1$, we only accept the new walk with probability q. This is determined by drawing a random number on the unit interval. If the random number is less than q, we reject the new walk and we hold on to the previous walk for the next iteration.

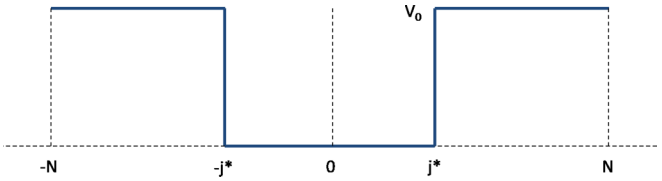

FIG. 1. Diagram depicting a finite square well of depth V_0 and ranging along on the one-dimensional lattice from $-j*$ to $j*$. The lattice itself ranges from $-N$ to N.

The expressions for the kinetic energy operator and the qp-qp correlation function G_1 in the classical isomorphism remain the same in the interacting system as that for the free particle. Paper 1 also derived a so-called atom-qp correlation function to study the effect of the presence of atoms on the lattice on the spread of the quantum particle. The atom-qp correlation function G_2 was defined in Paper 1 as

$$\hat{G}_2(n) = \sum_j n_j c^\dagger_{j+n} c_{j+n} \quad (21)$$

and its path integral estimator was determined to be

$$\Gamma_2(n) = \frac{1}{p}\sum_{\alpha=1}^{p} n_{j_{\alpha-n}}, \quad (22)$$

where, for a particular j_α, $n_{j_\alpha} = (0,1)$.

IV. PRESENCE OF ATOMS ON THE LATTICE IN A FIXED SQUARE WELL CONFIGURATION

A. Numerical solution for the square well configuration

Quantum mechanics textbooks, for instance Eisberg and Resnick [19], often consider the square well problem as one of the most basic and simple examples of demonstrating a solution to the Schrödinger equation having bound quantum states. In solving the square well problem for a continuous system, as they do, one has to consider the full set of possible energies $E > V_0$ and $E < V_0$, where V_0 is the depth of the potential well. Figure 1 shows a typical diagram for a one-dimensional square well configuration. For continuous systems, for $E > V_0$ the solutions to the Schrödinger equation turn out to be everywhere sinusoidal. The interacting quantum particle will be unbound in this region of energy. However, for $E < V_0$, it is found that the quantum particle will be trapped in the well and it will be confined to possess a set of discrete energies. The solutions for a particle in the well are complex exponentials and the solutions in the forbidden region, or the region outside the well, are real exponentials.

In this paper, we numerically solve the Schrödinger equation for a one-dimensional square well configuration for a discrete system, i.e., one where the locations of the qp and the classical atoms are confined to be on sites of a one-dimensional regular lattice. Let us set up the Schrödinger equation for this system. Because this is a discrete problem, we employ the Schrödinger difference equation. The difference form of the Schrödinger equation can be expressed compactly in the form

of a $(2N+1)\times(2N+1)$ matrix:

$$\mathbf{M}=\begin{pmatrix}
2+a & -1 & 0 & 0 & 0 & 0 & 0 & 0 & 0 & 0 & 0 & 0 & -1\\
-1 & 2+a & -1 & 0 & 0 & 0 & 0 & 0 & 0 & 0 & 0 & 0 & 0\\
0 & -1 & 2+a & -1 & 0 & 0 & 0 & 0 & 0 & 0 & 0 & 0 & 0\\
 & & & \ddots & & & & & & & & & \\
0 & 0 & 0 & -1 & 2+a & -1 & 0 & 0 & 0 & 0 & 0 & 0 & 0\\
0 & 0 & 0 & 0 & -1 & 2+b & -1 & 0 & 0 & 0 & 0 & 0 & 0\\
0 & 0 & 0 & 0 & 0 & -1 & 2+b & -1 & 0 & 0 & 0 & 0 & 0\\
 & & & & & & & \ddots & & & & & \\
0 & 0 & 0 & 0 & 0 & 0 & 0 & -1 & 2+b & -1 & 0 & 0 & 0\\
0 & 0 & 0 & 0 & 0 & 0 & 0 & 0 & -1 & 2+b & -1 & 0 & 0\\
0 & 0 & 0 & 0 & 0 & 0 & 0 & 0 & 0 & -1 & 2+a & -1 & 0\\
 & & & & & & & & & & & \ddots & \\
-1 & 0 & 0 & 0 & 0 & 0 & 0 & 0 & 0 & 0 & 0 & -1 & 2+a
\end{pmatrix}.$$

Let us define the range of j such that $-N \leqslant j \leqslant N$. Also, we can write

$$M_{ii} = 2+b, \quad -j^* \leqslant j \leqslant j^*, \tag{23}$$

$$M_{ii} = 2+a, \quad -N \leqslant j < -j^*, \quad \text{and} \quad j^* < j \leqslant N, \tag{24}$$

where the extent of the square well is from $-j^*$ to j^* inclusive. In this problem it is assumed that $a > b$.

Using *Mathematica* we solved for the eigenvalues and corresponding eigenvectors of the above matrix. We find that in general there are w energies in a lower band bound by the values $b \leqslant E \leqslant b+4.0$ and the remaining $2N+1-w$ energies are confined in a band bound by $a \leqslant E \leqslant a+4.0$.

B. Analytical statistical mechanics of the square well

Knowing the set of allowed discrete energies from solving for the eigenvalues of the above matrix, we can then directly employ the fundamental equations of statistical mechanics in the canonical ensemble to determine the values of some major equilibrium quantities for given inverse temperature β. The following are some of these fundamental formulas.

1. Partition function

$$Z = \sum_{\nu} e^{-\beta E_\nu}. \tag{25}$$

2. Average energy

$$\langle E\rangle = \frac{\sum_\nu E_\nu e^{-\beta E_\nu}}{Z}. \tag{26}$$

3. Average potential energy

In the canonical ensemble, the probability that the system is in a state ν is given by

$$P_\nu = \frac{e^{-\beta E_\nu}}{Z}. \tag{27}$$

The average potential energy in a state ν is given by

$$\langle V\rangle_\nu = \frac{\sum_j \Psi_j{}^* V \Psi_j}{\sum_j |\Psi_j|^2}. \tag{28}$$

In this paper, the potential configuration for both the numerical calculations and the PIMC computations is as follows:

$$V = \begin{cases} 0.0 & -j^* \leqslant j \leqslant j^*, \\ 10.0 & -N \leqslant j < -j^* \text{ and } j^* < j \leqslant N. \end{cases} \tag{29}$$

In processing Eqs (28) and (29) with the numerically determined eigenfunctions, we find that, except for low inverse temperature β, the average potential energy is

$$\langle V\rangle \approx 0.0. \tag{30}$$

Physically, this indicates that the qp is almost entirely within the square well, since the floor energy within the well was set to a value of 0.0 in all numerical calculations in this paper. The Monte Carlo solution closely matched the numerical solution across all β, which provides yet another demonstration for the power of this PIMC method.

4. Density matrix

In quantum statistical mechanics, one is typically interested in calculating the density matrix [21]. The density matrix describes a quantum system in a mixed state, as opposed to one in a pure state, which would simply be described by a single state vector. The density matrix is a quantum-mechanical analog to the phase-space probability in classical statistical mechanics. Explicitly, suppose that a given state $|\psi\rangle$ may be found in state $|\psi_1\rangle$ with probability p_1, in state $|\psi_2\rangle$ with probability $p_2, \ldots$, and in state $|\psi_n\rangle$ with probability p_n. The

density operator for this system is then [21]

$$\hat{\rho} = \sum_i p_i |\psi_i\rangle\langle\psi_i|. \tag{31}$$

By choosing a basis $|u_m\rangle$, which does not even need to be orthogonal, one may resolve the density operator into a density matrix, which has the matrix elements

$$\rho_{mn} = \sum_i p_i \langle u_m|\psi_i\rangle\langle\psi_i|u_n\rangle. \tag{32}$$

Then, for a given operator $\hat{A}$, the expectation value $\langle A\rangle$ is given by

$$\langle A\rangle = \sum_i p_i \langle\psi_i|\hat{A}|\psi_i\rangle = \sum_n \langle u_n|\hat{\rho}\hat{A}|u_n\rangle = \mathrm{Tr}(\hat{\rho}\hat{A}). \tag{33}$$

The expectation value of A for the mixed state is the sum of the expectation values of each of the pure states $|\psi_i\rangle$ weighted by probabilities p_i.

For any atomic configuration, the density matrix is an important mathematical object to calculate. In the case of a configuration of atoms on a one-dimensional lattice, the density matrix can be employed to provide a correlation function for the quantum particle. First we compute the density matrix for the square well configuration.

We write

$$\rho = \langle\phi^*(\mathbf{x})\phi(\mathbf{x}')\rangle = \frac{\sum_\nu \phi_\nu^*(\mathbf{x})\phi_\nu(\mathbf{x}')e^{-\beta E_\nu}}{Z}.$$

Expressing this relation in the formalism of the lattice, we write

$$\langle\phi^*(j)\phi(j')\rangle = \frac{\sum_{\nu(\text{states})} \phi_{\nu,j}^*\phi_{\nu,j'}e^{-\beta E_\nu}}{Z}.$$

For the subject square well problem, the density matrix can explicitly be written as

$$D_{jj'} = \frac{\sum_\nu \Psi_{\nu,j}^*\Psi_{\nu,j'}e^{-\beta E_\nu}}{\sum_\nu e^{-\beta E_\nu}}, \tag{34}$$

where the $\Psi_{\nu,j}$ are the numerically determined eigenfunctions of the Schrödinger difference equation indexed by ν.

5. qp-qp correlation function

The qp-qp correlation function is a function of atomic spacing n for any atomic configuration on a lattice and can be computed from the density matrix $D_{jj'}$ as

$$G_1(n) = \sum_{j=-N}^{N} D_{j,j+n}. \tag{35}$$

The purpose of G_1 is to provide a measure for the spread of the quantum particle on the lattice. Computationally, the wraparound restriction is enforced by subtracting $2N-1$ from $j+n$ if $j+n \geqslant N$.

6. Atom-qp correlation function

The atom-qp correlation function is a function of atomic spacing n for any atomic configuration on a lattice and can be computed from the density matrix $D_{jj'}$ as

$$G_2(n) = \sum_{j=-N}^{N} n_j D_{j+n,j+n}. \tag{36}$$

The factor n_j is 1 if site j is occupied by an atom and 0 otherwise.

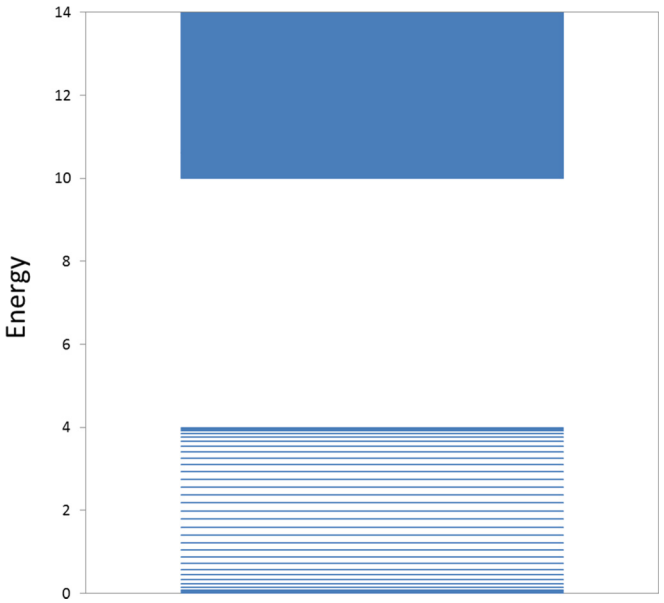

FIG. 2. Energy level diagram as determined by finding the eigenvalues of the matrix M for the Schrödinger difference equation for a well of width $w = 31$. In this case, $j^* = 15$, $a = 10.0$, and $b = 0.0$.

7. Radius of gyration

In general, in polymer physics, the radius of gyration is a measure of the spatial extent of a polymer chain. The path integral is isomorphic to a ring polymer, so the radius of gyration gives the effective radius of such a polymer. By definition, the radius of gyration is given by [22]

$$R = \sqrt{\frac{1}{p}\sum_{j=1}^{p}(\mathbf{r_j} - \bar{r})^2}, \tag{37}$$

where p is the number of steps in the polymer chain and $\mathbf{r_j} - \bar{r}$ is the distance from the jth bead on the chain and the center-of-mass position of the polymer.

C. Comparison of numerical calculations and computational results for square well configuration

Figures 2 through 4 are the energy level diagrams for the square well configuration for well widths $w = 31$, $w = 71$, and $w = 201$, respectively, as determined by solving the eigenvalues of the matrix M for the Schrödinger difference equation displayed previously. For each configuration, parameters a and b were 10.0 and 0.0, respectively, thus making the on-site potential $\epsilon = 10.0$ throughout, since $a = b + \epsilon$. To accomplish a well width of $w = 31$, we set j^* to 15, since the well ranges from $-j^*$ to j^*, including $j = 0$. Likewise, to

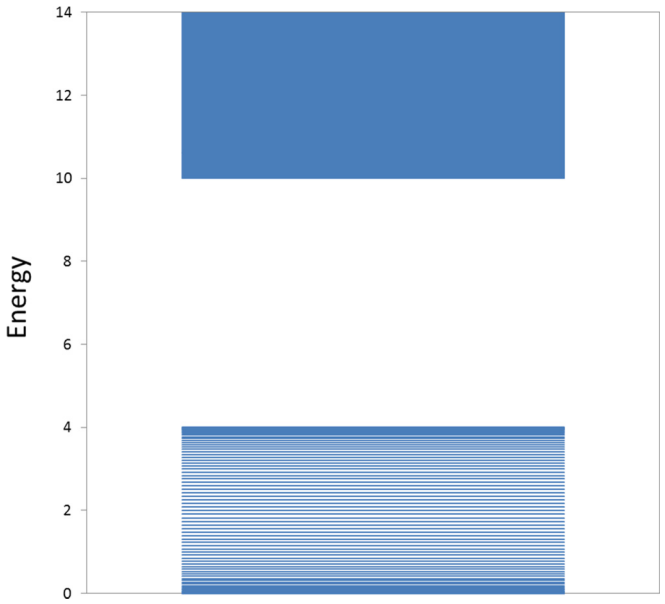

FIG. 3. Energy level diagram as determined by finding the eigenvalues of the matrix M for the Schrödinger difference equation for a well of width $w = 71$. In this case, $j^* = 35$, $a = 10.0$, and $b = 0.0$.

attain a well width of $w = 71$, we set j^* to 35, and to attain a well width of $w = 201$, we set j^* to 100. It turns out that the energy levels occur in two bands, one in $b \leqslant E \leqslant b + 4.0$ and one in $a \leqslant E \leqslant a + 4.0$. So, for the values of parameters a and b selected, the energy levels occur between $0.0 \leqslant E \leqslant 4.0$ and $10.0 \leqslant E \leqslant 14.0$. We also observe that the number of energy levels in the lower band is w, and the number in the upper energy band is $2N + 1 - w$, where the total number

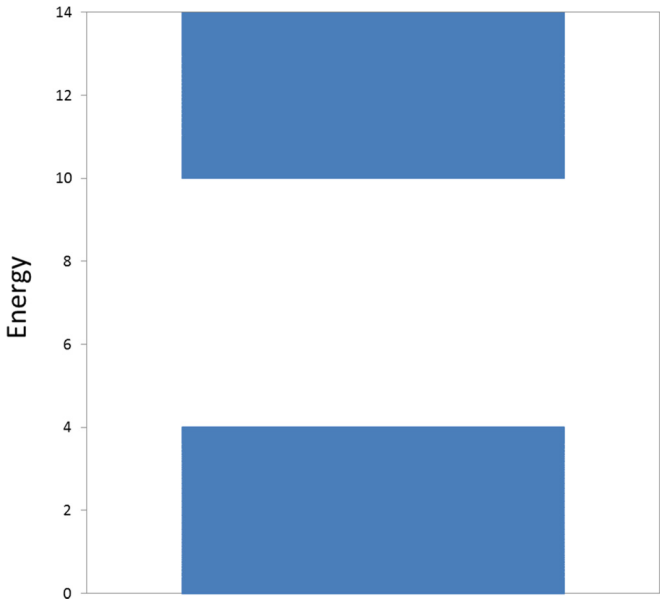

FIG. 4. Energy level diagram as determined by finding the eigenvalues of the matrix M for the Schrödinger difference equation for a well of width $w = 201$. In this case, $j^* = 100$, $a = 10.0$, and $b = 0.0$.

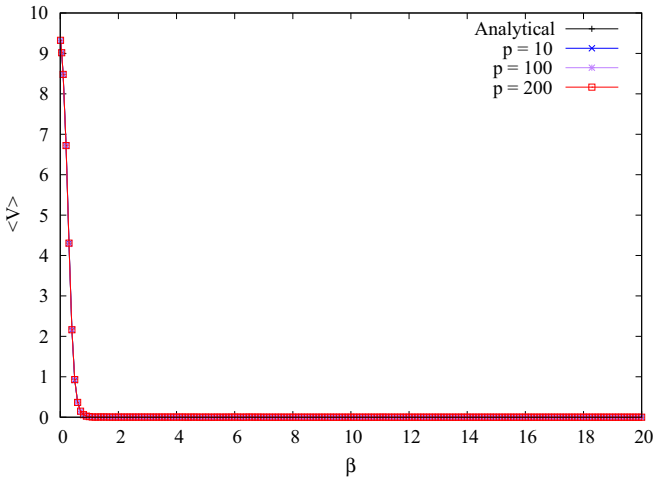

FIG. 5. Average potential energy versus inverse temperature, β, for a quantum particle moving on a one-dimensional lattice with a square well configuration of width $w = 31$, depth $\epsilon = 10.0$, and centered at the midpoint of the lattice. The numerical curve is a plot of the theoretical results. The other curves represent the Monte Carlo simulations for $p = 10$, $p = 100$, and $p = 200$. The agreement is strong. Error bars are too small to be seen on this scale.

of lattice sites is $2N + 1$, which is 501 for this paper. For instance, the number of energy levels in the lower band for the well of width 31 is 31, while the number in the upper band is $501 - 31 = 470$. We see that the wider the well, the more energy levels one observes in the lower band. We next primarily discuss well width $w = 31$ in detail and compare corresponding $w = 71$ and $w = 201$ results along the way. We show plots of the average potential energy vs β, the radius of gyration vs β, the qp-qp correlation function G_1 vs spacing n for a wide range of β, and the atom-qp correlation function G_2 vs spacing n for the same wide range of β. Each of these plots will compare computational graphs for number of steps $p = 10$, 100, and 200. Furthermore, each of these plots except the radius of gyration has a numerical curve for comparison.

Figures 5 and 6, 9 through 15, and 18 through 24 show direct comparisons between the numerical calculations and the Monte Carlo simulations for the square well configuration for well width $w = 31$. As can be seen in these plots, there was generally good agreement between the numerical and computational results. Monte Carlo runs were performed for the cases of the number of steps in the random walk being 10, 100, and 200. For all cases, the size of the one-dimensional lattice was 501 sites, where the central 31 sites represent the square well itself and have a floor energy of 0.0 in the units of this problem, whereas the other sites are $\epsilon = 10.0$ higher with an on-site potential of 10.0. The central 31 sites are not occupied by classical atoms, whereas the other sites are occupied by one classical atom. The inverse temperature β was varied extensively from 0.01 to 20.0 in the appropriate units. Furthermore, all computational plots are the result of running the PIMC code for 10^6 iterations. This number of iterations was selected based on keeping track of the evolution of the average kinetic energy across the range of inverse temperatures and ensuring that the average kinetic energy converged to within at least three decimal places.

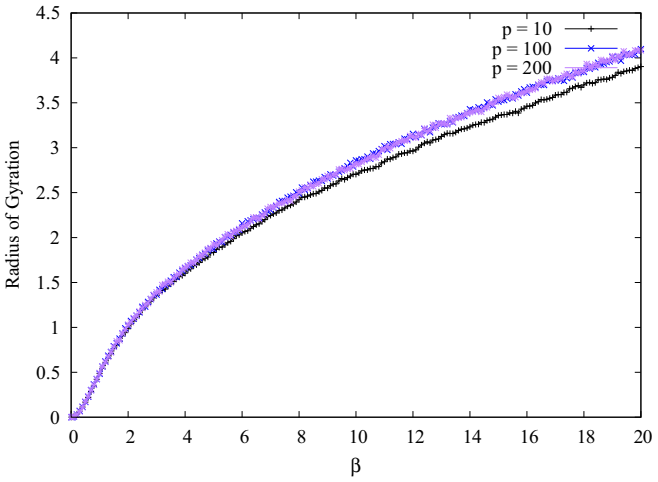

FIG. 6. Radius of gyration versus inverse temperature, β, for a quantum particle moving on a one-dimensional lattice with a square well configuration of width $w = 31$, depth $\epsilon = 10.0$, and centered at the midpoint of the lattice. The curves represent the Monte Carlo simulations for $p = 10$, $p = 100$, and $p = 200$. Error bars are too small to be seen on this scale.

Figure 5 is a plot of the average potential energy $\langle V \rangle$ as a function of the inverse temperature β, where β ranges from $\beta = 0.01$ through $\beta = 20.0$. This plot shows the graphs of the numerical average potential energy as well as the computational average potential energy for $p = 10$, $p = 100$, and $p = 200$, where all of these graphs are in the context of the square well potential configuration with $w = 31$. Equation (30) predicts that the average numerical potential energy has a theoretical value of 0.0 for $\beta > 0.10$. Figure 5 shows excellent agreement of the computational results with this numerical prediction once the inverse temperature β was high enough for the PIMC code to work effectively. This plot is further confirmation that the qp is almost entirely within the square well, since its potential energy is consistently close to the floor energy within the well. For well widths $w = 71$ and $w = 201$, the numerical and computational plots of the average potential energy versus β (not included) look almost identical to Fig. 5.

Figure 6 is a plot of the radius of gyration versus inverse temperature β for $w = 31$. Recall that the radius of gyration is a measure of the extent of the random walk on the lattice. The radius of gyration gradually increases with inverse temperature β and it is near zero when β is near zero and it grows to be approximately 4 for $\beta \approx 20.0$. So, even at large β, the random walk is very localized. This relatively small radius of gyration indicates that the extent of the random walk is much smaller than the dimension of the lattice as a whole, and, in particular, the square well portion of the potential configuration for any of the well widths considered. Also, with such a small radius of gyration for any β considered, we furthermore expect relatively narrow qp-qp correlation functions. Additionally, the corresponding plots for the radius of gyration for well widths $w = 71$ and $w = 201$ (not included) are almost identical to Fig. 6. The radius of gyration appears to be insensitive to the well width chosen.

Figure 7 is a plot of a sample density matrix for $\beta = 0.10$ and $w = 31$. This density matrix plot is displayed such that

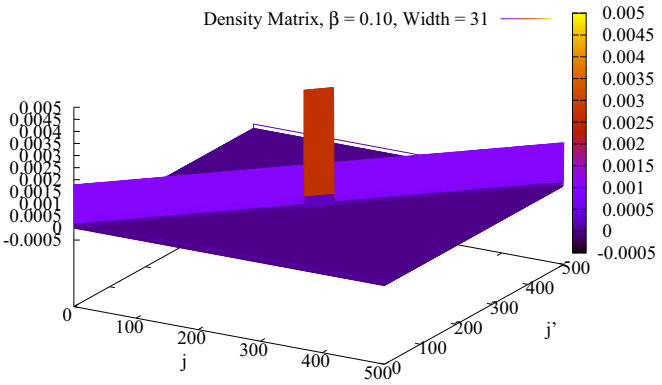

FIG. 7. 2D plot of a sample density matrix, which is for a well of width $w = 31$ and for $\beta = 0.10$. Note that the entire density matrix is practically zero except a line representing the diagonal elements, with particular concentration of relatively higher values near the center of the well.

j and j' range from 0 to 500, when in the calculations they actually range from -250 to 250. As can be clearly seen, most of the density matrix elements have values near zero. The only density matrix elements that possess substantial values are along a line representing the main diagonal with the highest values concentrated near the center of the well. Figure 8 shows the same plot but for a higher value of β, namely $\beta = 5.0$. We can see that for higher β, the raised line in the density matrix plot along the main diagonal disappeared, and the concentration of higher values of $D[j][j']$ occurring near the center of the well took on relatively larger values.

Figures 9 through 15 show the qp-qp correlation function for increasing inverse temperature β for the square well configuration for $w = 31$, including $\beta = 0.01$, $\beta = 0.05$, $\beta = 0.10$, $\beta = 0.50$, $\beta = 1.0$, $\beta = 5.0$, and $\beta = 10.0$. As the inverse temperature increases, i.e., as the temperature decreases, the qp-qp correlation function gets wider and wider. The qp-qp correlation function is a measure of the spread of the random walk in configuration space. For small β, like

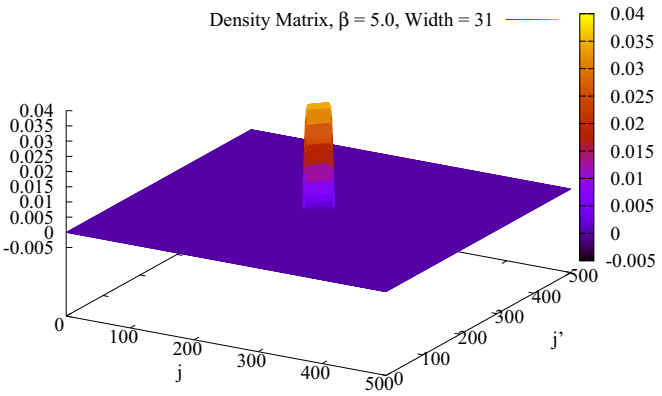

FIG. 8. 2D plot of a sample density matrix for a well of width $w = 31$ and for $\beta = 5.0$, which is a significantly higher value of β than that for Fig. 7. This density matrix for higher β is showing practically the entire matrix to be zero except for a small region near the center of the well.

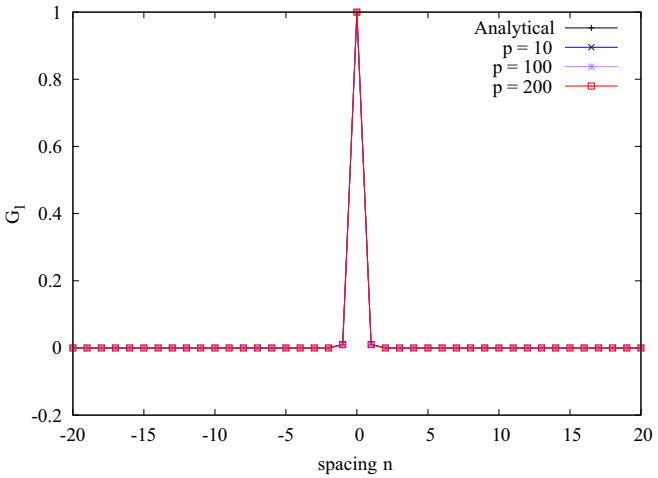

FIG. 9. The numerical and computational self-correlation (or qp-qp correlation) function $G_1(n)$ of the qp on the lattice with the subject square well configuration for a well of width $w = 31$ and for $\beta = 0.01$. The computational $G_1(n)$ is for $p = 10$, $p = 100$, and $p = 200$.

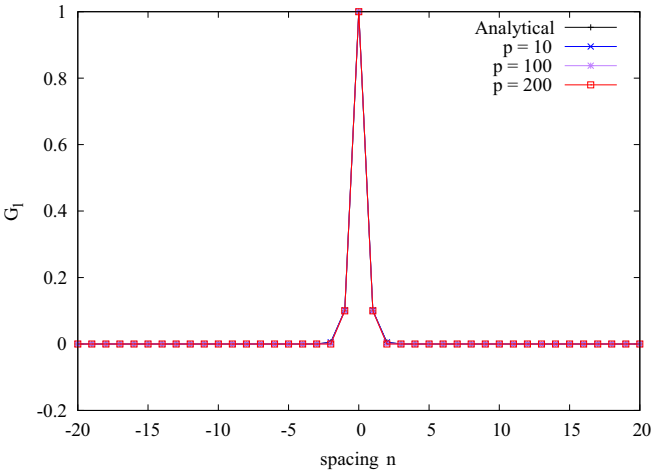

FIG. 11. The numerical and computational self-correlation (or qp-qp correlation) function $G_1(n)$ of the qp on the lattice with the subject square well configuration for a well of width $w = 31$ and for $\beta = 0.10$. The computational $G_1(n)$ is for $p = 10$, $p = 100$, and $p = 200$.

$\beta = 0.01$ and $\beta = 0.05$, the qp-qp correlation function is very narrow, indicating that the qp has mostly step sizes of 0 and 1 and nothing greater than these values. As β increases, the occurrence of larger step sizes becomes more frequent. Recall that the selection of step sizes is based on the conditional probability equation, Eq. (16), which directly depends on β.

Equation (16) also depends on the number of steps in the random walk, p. Unlike the average potential energy which seems to be independent of p, the qp-qp correlation function strongly depends on p. Across Figs. 9 through 15, we see that agreement of the computational qp-qp correlation graphs and the corresponding numerical graph is inversely proportional to p. This behavior is also determined by the conditional probability equation, Eq. (16), but it is not clear as to why this trend is true. This tendency is counterintuitive with experience with the path integral in other problems where improvement in calculating a parameter occurs for larger values of the number of steps [21]. We do not yet have a definitive answer as to why lowering the number of steps in the random walk improves the qp-qp correlation function for the square well problem.

One other comment applies to the plots of the qp-qp correlation function for the square well configuration for $w = 31$. For the correlation plots for the highest inverse temperature β considered, $\beta = 5.0$ and $\beta = 10.0$, Figs. 14 and 15, we see that there are some stray data points near the shoulders of the correlation graphs for $p = 100$ and $p = 200$. Again, the qp-qp correlation graphs for $p = 10$ always agree

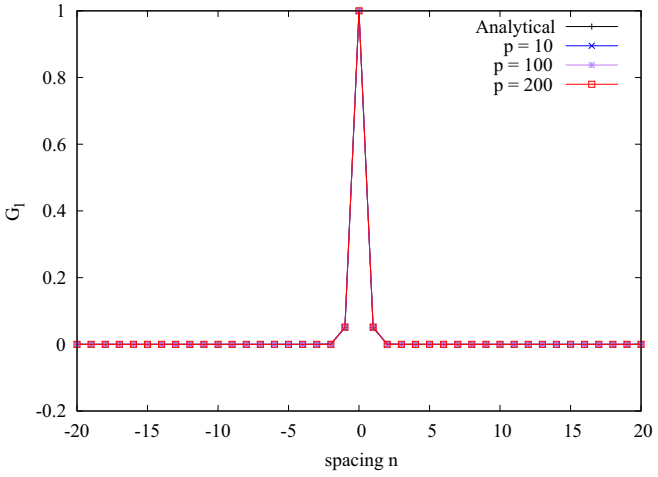

FIG. 10. The numerical and computational self-correlation (or qp-qp correlation) function $G_1(n)$ of the qp on the lattice with the subject square well configuration for a well of width $w = 31$ and for $\beta = 0.05$. The computational $G_1(n)$ is for $p = 10$, $p = 100$, and $p = 200$.

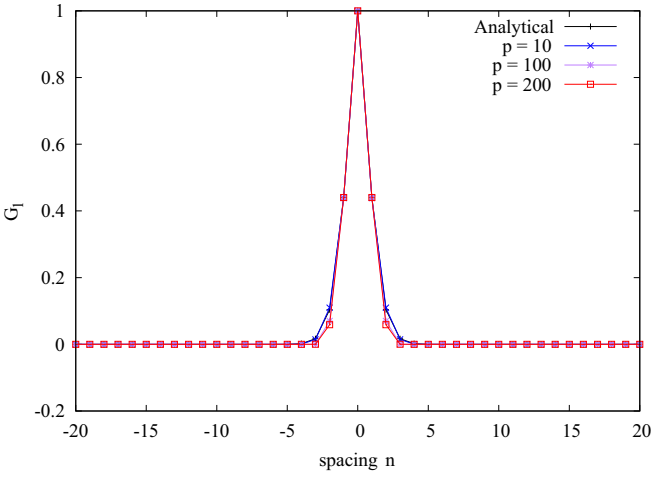

FIG. 12. The numerical and computational self-correlation (or qp-qp correlation) function $G_1(n)$ of the qp on the lattice with the subject square well configuration for a well of width $w = 31$ and for $\beta = 0.50$. The computational $G_1(n)$ is for $p = 10$, $p = 100$, and $p = 200$.

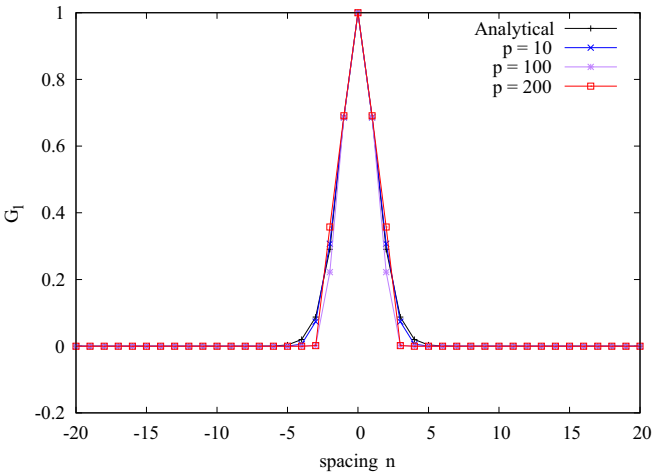

FIG. 13. The numerical and computational self-correlation (or qp-qp correlation) function $G_1(n)$ of the qp on the lattice with the subject square well configuration for a well of width $w = 31$ and for $\beta = 1.0$. The computational $G_1(n)$ is for $p = 10$, $p = 100$, and $p = 200$.

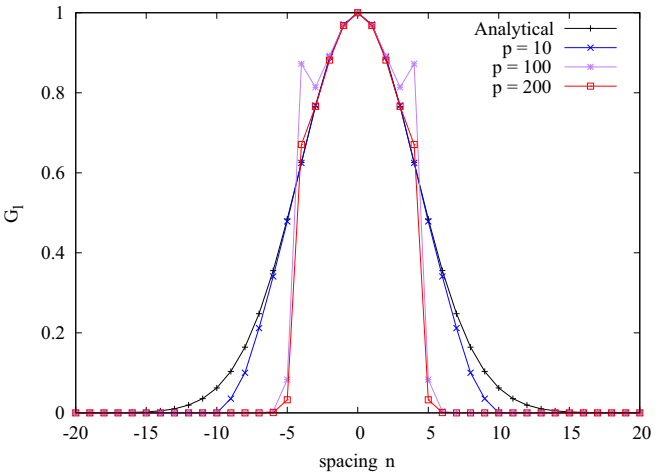

FIG. 15. The numerical and computational self-correlation (or qp-qp correlation) function $G_1(n)$ of the qp on the lattice with the subject square well configuration for a well of width $w = 31$ and for $\beta = 10.0$. The computational $G_1(n)$ is for $p = 10$, $p = 100$, and $p = 200$.

with the numerical solution the best, but the plots for the larger p for higher β are showing these additional errors.

For well widths $w = 71$ and $w = 201$, for all β, the widths of the central peak for the numerical, $p = 10$, $p = 100$, and $p = 200$ graphs were comparable with their $w = 31$ counterparts. As usual, the numerical and $p = 10$ plots were consistently wider than the $p = 100$ and $p = 200$ plots. Also, for the high-β plots, i.e., $\beta = 5.0$ and $\beta = 10.0$, the $p = 100$ and $p = 200$ plots for $w = 71$ and $w = 201$ exhibited the same extraneous points near the shoulders as did their $w = 31$ counterparts. It is furthermore interesting that the widths of the central peaks do not seem to depend on the well widths chosen, and this makes sense because these well widths are significantly larger than the radii of gyration for the random walk in this problem. Figures 16 and 17 are the plots for the numerical and computational qp-qp correlation function for $\beta = 10.0$ and for $w = 71$ and $w = 201$, respectively. Like the other qp-qp correlation plots for $w = 71$ and $w = 201$, they very closely agree with their $w = 31$ counterparts. Because of the errors in the shoulders of the plots being most dramatic for $\beta = 10.0$, we include these plots just to show their slight differences.

Figures 18 through 24 show the numerical atom-qp correlation graph along with the computational graphs for $p = 10$, $p = 100$, and $p = 200$ for the square well with $w = 31$ for the same values of the inverse temperature β as was considered for studying the qp-qp correlation function. As expected, these plots plateau for a spacing equal to the well width, which is 31 in this case. It is interesting to note that for smaller β,

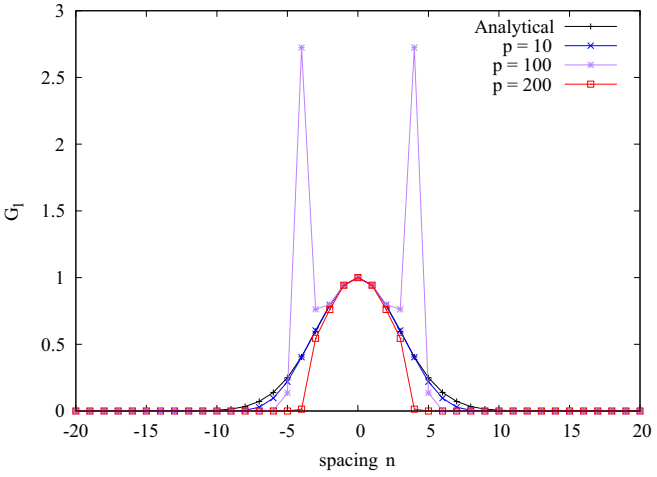

FIG. 14. The numerical and computational self-correlation (or qp-qp correlation) function $G_1(n)$ of the qp on the lattice with the subject square well configuration for a well of width $w = 31$ and for $\beta = 5.0$. The computational $G_1(n)$ is for $p = 10$, $p = 100$, and $p = 200$.

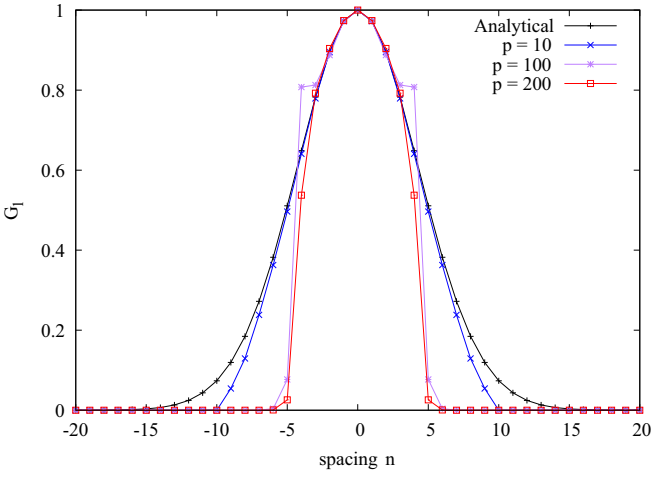

FIG. 16. The numerical and computational qp-qp correlation function $G_1(n)$ of the qp on the lattice with the subject square well configuration for a well of width $w = 71$ and for $\beta = 10.0$. The computational $G_1(n)$ is for $p = 10$, $p = 100$, and $p = 200$.

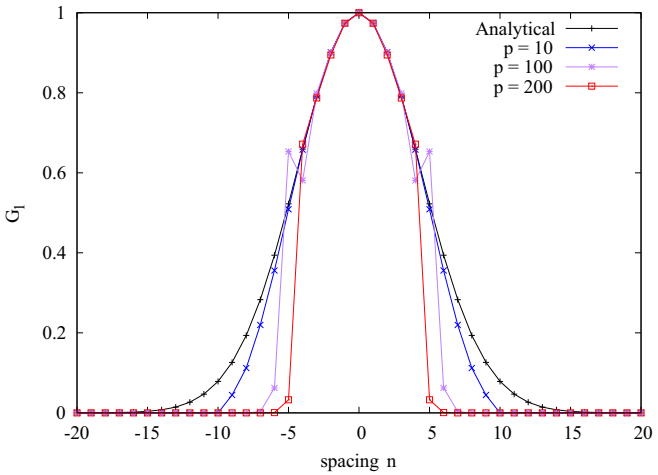

FIG. 17. The numerical and computational qp-qp correlation function $G_1(n)$ of the qp on the lattice with the subject square well configuration for a well of width $w = 201$ and for $\beta = 10.0$. The computational $G_1(n)$ is for $p = 10$, $p = 100$, and $p = 200$.

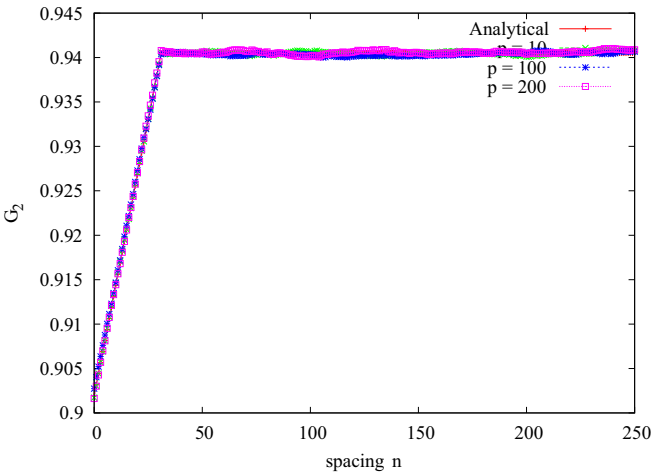

FIG. 19. The numerical and computational atom-qp correlation function $G_2(n)$ of the qp on the lattice with the subject square well configuration for a well of width $w = 31$ and for $\beta = 0.05$. The computational $G_2(n)$ is for $p = 10$, $p = 100$, and $p = 200$.

like $\beta \leqslant 0.10$, the plateau is slightly below $G_2 = 1.0$, but for higher β the plateau is firmly set at $G_2 = 1.0$ and the numerical atom-qp correlation graph does not seem to be affected by temperature at all. The numerical atom-qp correlation graph appears invariant across the range of $\beta > 0.10$ considered, as can be seen by comparing Figs. 21 through 24 with each other. This is best understood by knowing the properties of the density matrix. First, the sum of all diagonal elements equals 1. Equation (36) gives the form of the atom-qp correlation function $G_2(n)$. As can be seen, each term in the sum is a diagonal element of the density matrix, where each element is multiplied by $n_j = 1$ if an atom exists at its corresponding location j; otherwise, it is multiplied by $n_j = 0$. This result can be understood as the product of two functions. The first is n_j as a function of j. This is a step function where its value is 0 for $-j^* \leqslant j \leqslant j^*$ and 1 otherwise. For each term in the nth sum $G_2(n)$, this step function is multiplied by $D_{j+n,j+n}$. As can be seen in Fig. 8, even though the sum of the diagonal elements of the density matrix is 1, all of the substantial values for $D_{j,j'}$ are in the vicinity of the well, i.e., near the center of the plane shown in Fig. 8. If $n = 0$, the jth value of n_j corresponds to the jth value of $D_{j,j}$. Hence, for $G_2(0)$, the substantial elements in $D_{j,j}$ are all multiplied by 0, and so $G_2(0) \approx 0.0$. As n increases, there begins to be a misalignment between n_j and $D_{j+n,j+n}$, so that substantial elements near the center of the density matrix are then multiplied by $n_j = 1$. When $n \geqslant 2j^* + 1$, there is complete misalignment and all of the substantial elements of $D_{j+n,j+n}$ are multiplied by $n_j = 1$, and since these substantial elements sum to 1, this is why the G_2 plot plateaus to 1 for any $n \geqslant 2j^* + 1$, the well width. For lower β, we see the same behavior of G_2, but the plateau is at a value less than 1.0. If one studies Fig. 7,

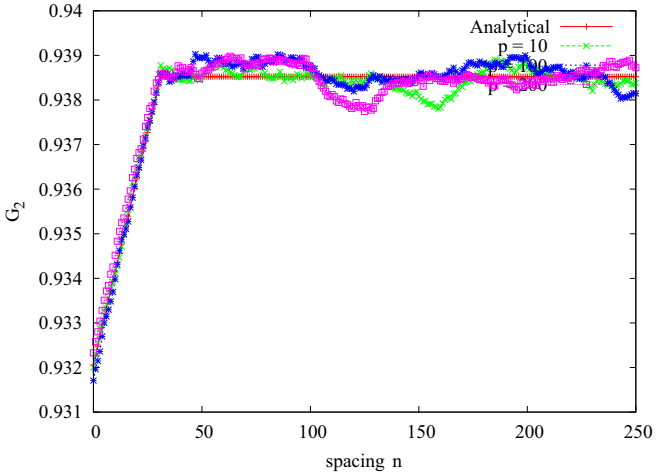

FIG. 18. The numerical and computational atom-qp correlation function $G_2(n)$ of the qp on the lattice with the subject square well configuration for a well of width $w = 31$ and for $\beta = 0.01$. The computational $G_2(n)$ is for $p = 10$, $p = 100$, and $p = 200$.

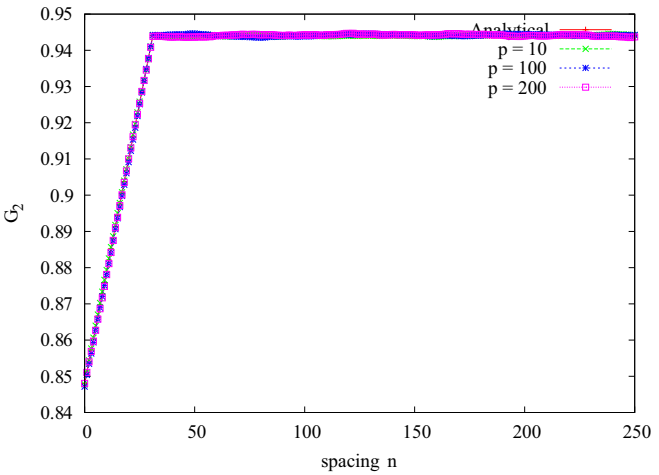

FIG. 20. The numerical and computational atom-qp correlation function $G_2(n)$ of the qp on the lattice with the subject square well configuration for a well of width $w = 31$ and for $\beta = 0.10$. The computational $G_2(n)$ is for $p = 10$, $p = 100$, and $p = 200$.

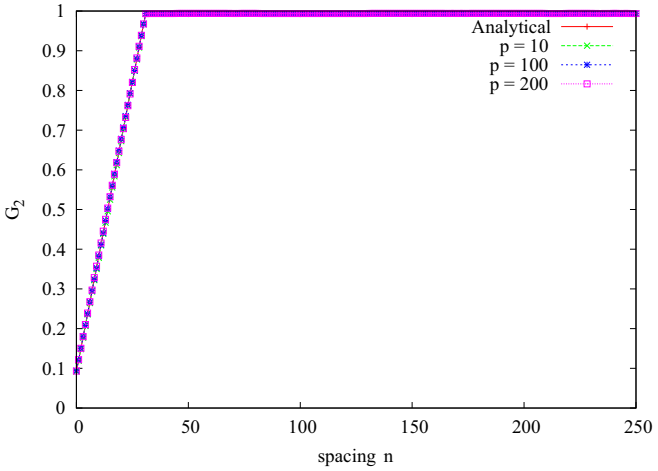

FIG. 21. The numerical and computational atom-qp correlation function $G_2(n)$ of the qp on the lattice with the subject square well configuration for a well of width $w = 31$ and for $\beta = 0.50$. The computational $G_2(n)$ is for $p = 10$, $p = 100$, and $p = 200$.

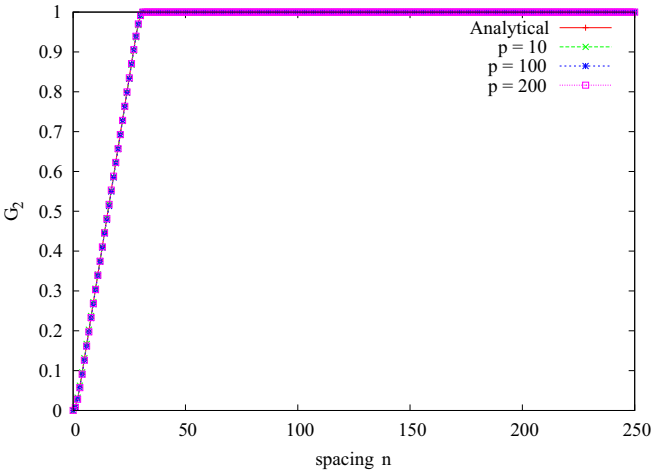

FIG. 23. The numerical and computational atom-qp correlation function $G_2(n)$ of the qp on the lattice with the subject square well configuration for a well of width $w = 31$ and for $\beta = 5.0$. The computational $G_2(n)$ is for $p = 10$, $p = 100$, and $p = 200$.

one sees that the substantial values of G_2 are still along the main diagonal and still sum to 1.0; however these substantial values of G_2 are spread along the main diagonal with a lower primary concentration near the center of the well. Therefore, even when the above-discussed misalignment is complete, the G_2 will sum to a value that is less than 1. Additionally, as in the case for the average potential energy, there appears to be an independence of the computational atom-qp correlation plot on the choice of p. In general, we see excellent agreement among all computational G_2 plots and the corresponding numerical G_2 plot across the entire range of inverse temperature β.

For well widths $w = 71$ and $w = 201$, the plots of the atom-qp correlation function versus spacing n are similar to their $w = 31$ counterpart. The only difference in the $w = 71$ and $w = 201$ atom-qp correlation plots is that their respective plateaus occur at $n = 71$ and $n = 201$. Figures 25 and 26 are plots for the atom-qp correlation function for $\beta = 10.0$ and for $w = 71$ and $w = 201$, respectively, and these plots have Fig. 24 as their $w = 31$ counterpart. Figures 25 and 26 were included just to show the general shape of the $w = 71$ and $w = 201$ atom-qp correlation functions with their different plateaus, which are equal to the corresponding well widths.

V. SUMMARY AND CONCLUSIONS

In this work we applied path integral Monte Carlo to the case of the bound and extended states of an equilibrated qp on a one-dimensional lattice. The qp experiences the periodic potential resulting from a quenched distribution of atoms. We study the particular case of a low-mass qp interacting with a set configuration of classical atoms on a one-dimensional lattice arranged such that all sites on the lattice are occupied by a

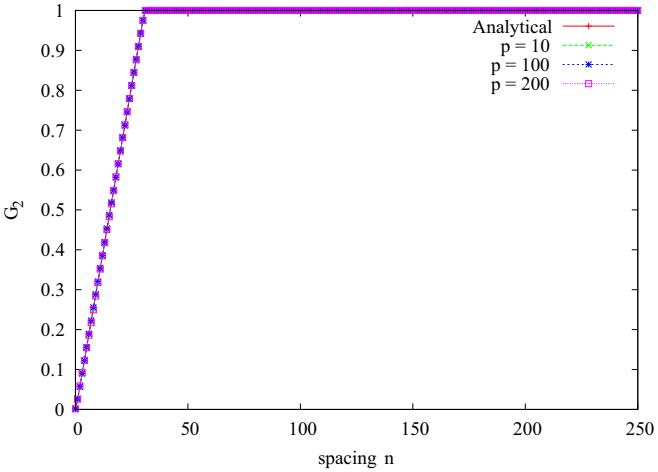

FIG. 22. The numerical and computational atom-qp correlation function $G_2(n)$ of the qp on the lattice with the subject square well configuration for a well of width $w = 31$ and for $\beta = 1.0$. The computational $G_2(n)$ is for $p = 10$, $p = 100$, and $p = 200$.

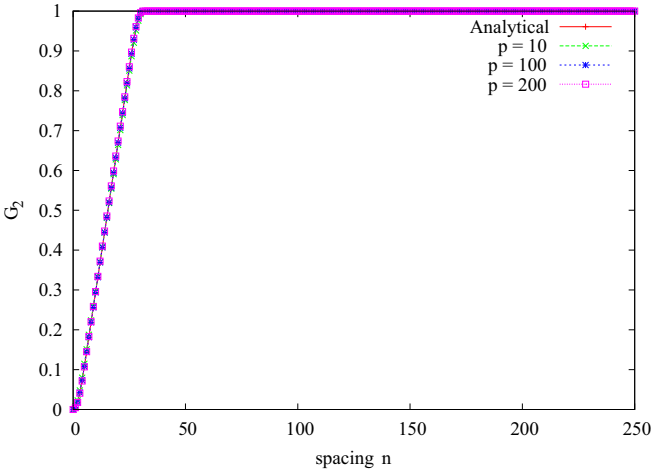

FIG. 24. The numerical and computational atom-qp correlation function $G_2(n)$ of the qp on the lattice with the subject square well configuration for a well of width $w = 31$ and for $\beta = 10.0$. The computational $G_2(n)$ is for $p = 10$, $p = 100$, and $p = 200$.

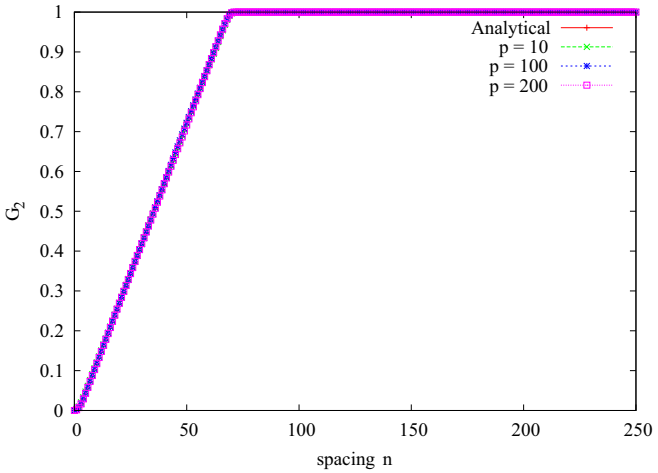

FIG. 25. The numerical and computational atom-qp correlation function $G_2(n)$ of the qp on the lattice with the subject square well configuration for a well of width $w = 71$ and for $\beta = 10.0$. The computational $G_2(n)$ is for $p = 10$, $p = 100$, and $p = 200$.

single atom except for a set expanse of sites about the center of the lattice which are unoccupied. This configuration produces a finite square well potential in one dimension, and the extent of this expanse is the well width. To be able to perform this study, we utilized a path integral Monte Carlo algorithm developed in O'Callaghan and Miller [3] specifically for this problem of a qp being confined to occupy lattice sites, as opposed to other path integral algorithms for continuous systems, and this same paper established a connection between the quantum trace and the weighted sum of variable-step-sized random walks on the lattice. This isomorphism was used to establish a method for carrying out Monte Carlo calculations of the thermal average of physical observables such as the partition function, kinetic energy, energy fluctuation, and self-correlation of the qp.

Using the same path integral Monte Carlo algorithm with Metropolis sampling, the system properties can be solved for a

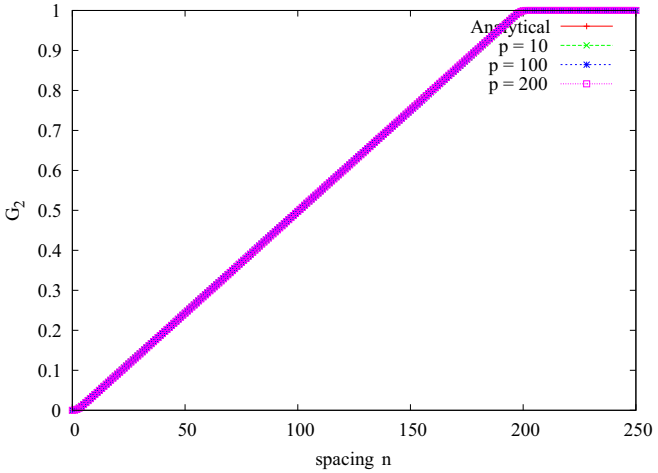

FIG. 26. The numerical and computational atom-qp correlation function $G_2(n)$ of the qp on the lattice with the subject square well configuration for a well of width $w = 201$ and for $\beta = 10.0$. The computational $G_2(n)$ is for $p = 10$, $p = 100$, and $p = 200$.

variety of atomic configurations. However, it is only possible to obtain an analytical solution to the Schrödinger equation for very few potentials. Our goal was to construct a nontrivial atomic configuration that could be input into the Monte Carlo code and also be solved numerically. Numerical computations were compared with corresponding Monte Carlo simulations and the agreement for the potential energy was within 1% across all β considered.

The success of the PIMC algorithm to calculate the potential energy was independent of the number of steps in the random walk, p. The corresponding agreement for the qp-qp correlation functions show that the numerical and computational results follow one another; however, the error is significantly more than what is observed for the potential energy. The discrepancy between the numerical and computational qp-qp correlation plots was least for $\beta \leqslant 0.10$ and it grew to be greatest for higher β. For $\beta \leqslant 0.10$, the error between the numerical and computational qp-qp correlation plots was within 1% for all p. However, as β increased, while the $p = 10$ plot continued to follow the numerical plot, the $p = 100$ and $p = 200$ plots began deviating significantly. For the highest β considered, i.e., $\beta = 10.0$, the $p = 10$ plot agreed with the numerical plot within 20%. On the other hand, for higher β, the $p = 100$ and $p = 200$ qp-qp correlation plots fared much worse, and in fact, they even exhibited extraneous high points in the shoulders of the central peak. This same disagreement in the qp-qp correlation function was also seen in Paper 1. Hence, we are seeing parallel behavior of the Monte Carlo algorithm for two totally different potentials, a one-dimensional square well in this paper and a one-dimensional striped configuration in Paper 1. It is important to see the general behavior of the PIMC algorithm for problems that can be solved analytically or numerically so that we can have expectation of behavior for future problems that cannot be solved analytically or numerically.

Finally, the agreement between the numerical and computational results for the atom-qp correlation function was within 1% for $\beta \geqslant 0.05$. We see some oscillatory behavior for the computational G_2 plots for $\beta = 0.01$. We also observed that the accuracy of the computational atom-qp correlation plots appeared to be independent of the number of steps in the random walk p.

In general, the PIMC approach seems to do very well for predictions of energy and atom-qp correlation and only fairly well for qp-qp correlation. Based on the success of the approach demonstrated here, we are planning to employ the path integral method to investigate additional quenched and annealed equilibrium ensembles. In particular, we plan to investigate situations where either Anderson localization or self-trapping of the qp plays the dominant role.

ACKNOWLEDGMENTS

One author (M.O.) appreciates the support received from the Lockheed Martin Corporation. The authors are grateful to Benjamin Janesko, Jim Mayne, Brian Nevius, Terrence Reese, Steven Pehrson, Douglas Abernathy, J. Michael Gibbs, George Gilbert, Ken Richardson, Igor Prokhorenkov, the TCU Computer Support Team, and the peer reviewers for this journal for their technical assistance.

[1] J. Hernandez, Rev. Mod. Phys. **63**, 675 (1991); D. Chandler and K. Leung, Annu. Rev. Phys. Chem. **45**, 557 (1994); G. N. Chuev, J. Exp. Theor. Phys. **88**, 807 (1999).

[2] For a review of both experimental and theoretical physics of positron annihilation in fluids, see I. T. Iakubov and A. G. Khrapak, Prog. Phys. **45**, 697 (1982).

[3] M. O'Callaghan and B. N. Miller, Phys. Rev. E **89**, 042124 (2014).

[4] H. Guo and B. N. Miller, J. Stat. Phys. **98**, 347 (2000).

[5] For a good explanation of the tight-binding model, see F. Dominguez-Adame and V. A. Malyshev, Am. J. Phys. **72**, 226 (2004).

[6] J. Ibanez-Azpiroz, A. Eiguren, A. Bergara, G. Pettini, and M. Modugno, Phys. Rev. A **87**, 011602(R) (2013); D. Witthaut, T. Salger, S. Kling, C. Grossert, and M. Weitz, *ibid.* **84**, 033601 (2011).

[7] J. K. Xue, A. X. Zhang, and J. Liu, Phys. Rev. A **77**, 013602 (2008); S. Paul and E. Tiesinga, *ibid.* **88**, 033615 (2013); A. A. Shams and H. R. Glyde, Phys. Rev. B **79**, 214508 (2009).

[8] J. T. Chalker, T. S. Pickles, and P. Shukla, Phys. Rev. B **82**, 104209 (2010).

[9] Y. Yao, F. Ye, X. L. Qi, S. C. Zhang, and Z. Fang, Phys. Rev. B **75**, 041401(R) (2007); M. P. Lopez-Sancho and M. C. Munoz, *ibid.* **83**, 075406 (2011); S. Fratini, D. Gosalbez-Martinez, P. Merodio Camera, and J. Fernandez-Rossier, *ibid.* **88**, 115426 (2013); M. Bellec, U. Kuhl, G. Montambaux, and F. Mortessagne, *ibid.* **88**, 115437 (2013); J. Gonzalez, F. Guinea, and J. Herrero, *ibid.* **79**, 165434 (2009); P. V. Buividovich and M. I. Polikarpov, *ibid.* **86**, 245117 (2012).

[10] I. Prigogine, *Advances in Chemical Physics, New Methods in Computational Quantum Mechanics* (Wiley-Interscience, New York, 1996).

[11] D. M. Ceperley, Rev. Mod. Phys. **67**, 279 (1995).

[12] There are several papers which demonstrate research utilizing path integrals on a lattice. However, no paper solves the path integral exactly as a product of modified Bessel functions. The following are some papers which employ path integrals on a lattice: R. J. Hinde, Chem. Phys. Lett. **418**, 481 (2006); R. Vidigal and R. Dickman, Braz. J. Phys. **118**, 1 (2005); M. Creutz and B. Freedman, Ann. Phys. **132**, 427 (1981); R. A. Sauerwein and S. Kais, Phys. Rev. E **64**, 056120 (2001); L. M. Sese, J. Chem. Phys. **139**, 044502 (2013); C. Predescu, J Theor. Comput. Chem. **05**, 255 (2006).

[13] Y. Yu, M. Han, and G. Gao, Phys. Chem. Chem. Phys. **3**, 437 (2001); M. Lee, C. McCabe, and P. T. Cummings, Fluid Phase Equilib. **221**, 63 (2004); A. Yethiraj and C. K. Hall, J. Chem. Phys. **95**, 8494 (1991); A. Lang, G. Kahl, C. N. Likos, H. Lowen, and M. Watzlawek, J. Phys.: Condens. Matter **11**, 10143 (1999); F. del Rio, O. Guzman, and A. Malijevsky, J. Phys. Chem. **99**, 1587 (1995); R. Fantoni, A. Giacometti, A. Malijevsky, and A. Santos, J. Chem. Phys. **131**, 124106 (2009).

[14] A. Czachor and P. Peczkowski, Phys. Part. Nuclei Lett. **8**, 542 (2011).

[15] H. Wu, D. W. L. Sprung, and J. Martorell, Phys. Rev. B **45**, 11960 (1992).

[16] A. Lomakin, N. Asherie, and G. B. Benedek, J. Chem. Phys. **104**, 1646 (1996).

[17] S. A. McCarthy, J. B. Wang, and P. C. Abbott, Comput. Phys. Commun. **141**, 175 (2001); E. Rasanen, H. Saarikoski, V. N. Stavrou, A. Harju, M. J. Puska, and R. M. Nieminen, Phys. Rev. B **67**, 235307 (2003); R. Ugajin, Physica B **253**, 96 (1998); Phys. Rev. B **53**, 6963 (1996); M. Califano and P. Harrison, J. Appl. Phys. **88**, 5870 (2000).

[18] T. B. Boykin and G. Klimeck, Eur. J. Phys. **26**, 865 (2005).

[19] R. Eisberg and R. Resnick, *Quantum Physics of Atoms, Molecules, Solids, Nuclei and Particles* (Wiley & Sons, New York, 1985).

[20] M. Abramowitz and I. A. Stegun, *Handbook of Mathematical Functions* (Dover, New York, 1965).

[21] R. P. Feynman, *Statistical Mechanics* (Westview Press, Boulder, CO, 1972).

[22] A. R. Khokhlov and A. Y. Grosberg, *Statistical Physics of Macromolecules (Polymers and Complex Materials)* (American Institute of Physics, Woodbury, NY, 1997).